Trans-species microRNA loci in the parasitic plant *Cuscuta campestris* have a U6-like snRNA promoter

Collin Hudzik[1,2], Sean Maguire[3], Shengxi Guan[3], Jeremy Held[2,4], and Michael J. Axtell[1,2]

1. Department of Biology, The Pennsylvania State University, University Park, PA, 16802, USA

2. Huck Institutes of the Life Sciences, The Pennsylvania State University, University Park, PA, 16802, USA

3. New England Biolabs, Inc., 240 County Road, Ipswich, MA 01938, USA

4. Department of Plant Pathology and Environmental Microbiology, The Pennsylvania State University, University Park, PA, 16802, USA

Corresponding Author: Michael J. Axtell, mja18@psu.edu

Abstract

Small regulatory RNAs can move between organisms during pathogenic interactions and regulate gene expression in the recipient. If and how such "*trans*-species" small RNAs are distinguished from normal small RNAs is not known. *Trans*-species microRNAs from the parasitic plant *Cuscuta campestris* are known to specifically accumulate at the haustorium, the organ that invades host plant stems. We find that haustorial accumulation of *trans*-species microRNAs has no host specificity, and can be replicated in haustoria stimulated to develop in the complete absence of a host. We also find that the loci encoding *C. campestris trans*-species microRNAs are distinguished by a common 10 base-pair *cis*-regulatory element. This element is identical to a previously described upstream sequence element used by all plant small nuclear RNA loci. The sequence context of this element strongly suggests U6-like transcription by RNA polymerase III. The element promotes accumulation of *trans*-species miRNAs in a heterologous system. This common promoter element distinguishes *C. campestris trans*-species microRNA loci from other plant small RNAs; other plant small RNA loci are transcribed by polymerases II or IV, and lack any common promoter motifs. Our data suggest that *C. campestris trans*-species miRNAs are produced in a manner distinct from canonical miRNAs. This distinct production may allow them to be exported to hosts.

Significance statement

Pathogens and parasites often manipulate their host's physiology and immune responses. One manipulation method is delivery of small regulatory RNAs into the host. The small RNAs target specific host messenger RNAs for degradation. There are numerous examples of such "*trans*-species" small RNAs, but little has been known about their genetic regulation. This study identifies a common promoter motif unique to the *trans*-species small RNA genes in the parasitic plant *Cuscuta campestris* (field dodder). This shows that the *trans*-species miRNAs are a distinct type of small RNA with a common transcriptional program. Targeting this common element may be a way to increase host resistance to *C. campestris*.

Introduction

Small regulatory RNAs are 21 to 24 nucleotide RNAs which play an important role as regulators of gene expression. Plants produce at least three distinct classes of small RNAs. MicroRNAs (miRNAs) are usually 21-22 nucleotides in length and derived from single-stranded stem-loop precursors (Chen, 2005; Axtell, 2013). MiRNAs usually regulate specific target mRNAs post-

transcriptionally. Canonical plant miRNAs are processed from longer primary transcripts. Canonical plant miRNA precursors in *Arabidopsis thaliana* are transcribed by RNA polymerase II, have variable lengths, and besides a TATA box (Xie et al., 2005) lack any common *cis* regulatory elements. There are also two distinct types of short interfering RNAs (siRNAs), both of which originate from double-stranded RNA precursors. Shorter siRNAs are 21-22 nucleotides long, and function outside of the nucleus in post-transcriptional silencing of endogenous mRNAs, aberrant RNAs, and viral RNA (Fei et al., 2013). Longer siRNAs are mostly 24 nucleotides long and function in the nucleus to direct *de novo* DNA methylation to transposons and other non-genic sequences (Matzke and Mosher, 2014). *Trans*-species small RNAs, defined as small RNAs that naturally move from one organism to another, play important roles in plant-pathogen interactions by targeting mRNAs in the recipient organism (Huang et al., 2019; Hudzik et al., 2020). Most experimentally verified cases involve miRNAs (Zhang et al., 2016; Shahid et al., 2018) or 21-22 nucleotide siRNAs (Weiberg et al., 2013; Cai et al., 2018; Hou et al., 2019).

Cuscuta campestris is an obligate parasitic plant which uses a specialized organ called the haustorium to pierce the host stem and fuse with the vasculature to feed (Heide-Jørgensen, 2008). The haustorium facilitates bidirectional movement of photosynthates and macromolecules between the host and parasite (Birschwilks et al., 2006; Roney et al., 2007; David-Schwartz et al., 2008; Kim and Westwood, 2015). Haustorium organogenesis is divided into the adhesive, intrusive, and conductive phases (Shimizu and Aoki, 2019). During the adhesive phase, cortical cells from the parasite stem begin to differentiate and divide to form the endophyte primordia. Digitate cells from the endophyte primordia eventually extend through and invade the host stem, marking the transition into the intrusive phase. Digitate cells, now referred to as searching hyphae, continue to extend and move in-between cortical cells to identify the host's vasculature (Vaughn, 2003). Searching hyphae will differentiate into xylic or phloic hyphae once in contact with the respective vasculature. Haustoria have fully matured and reached the conductive phase once differentiated hyphae begin to actively receive nutrients from the host (Vaughn, 2006).

C. campestris produces a set of miRNAs specifically at the interface between the host and parasite (Shahid et al., 2018; Johnson et al., 2019), some of which can move long distances in the host plant (Subhankar et al., 2021). Several interface-induced miRNAs from *C. campestris* have been experimentally demonstrated to target and regulate host mRNAs, and thus act in a *trans*-species manner. Host mRNAs involved in biotic defense, hormone signaling, and vascular development are targeted (Shahid et al., 2018; Johnson et al., 2019). A subset of the interface-induced, *trans*-species miRNAs are 22 nucleotides long, which allows for production host-derived secondary siRNAs to accumulate during parasitism (Chen et al., 2010; Cuperus et al., 2010). Analysis of interface-induced miRNA diversity within and between *Cucuta* species provides clear evidence that several miRNA-target relationships have been under selection (Johnson et al., 2019). When *C. campestris* is grown on a host plants with a non-functional copy of certain targets parasite biomass increases significantly (Shahid et al., 2018). Thus we hypothesize that *C. campestris* uses interface-induced miRNAs to manipulate host gene expression to increase parasite fitness. We use the term "interface-induced miRNAs" to refer to all such differentially expressed miRNAs because not all of them have been directly proven to target host mRNAs.

In this study we examine the regulation of *C. campestris* interface-induced miRNAs with respect to haustorial development and host identity. We also analyze *cis*-regulatory features found at the loci encoding *C. campestris* interface-induced miRNAs.

Results

Improved annotation of interface-induced *MIRNA* loci from *C. campestris*

A total of 43 *C. campestris* interface-induced *MIRNA* loci, representing 36 distinct families, were previously identified based on a single small RNA-seq experiment with two biological replicates per tissue type. Subsequently several more small RNA-seq datasets from *C. campestris* infestation of *A. thaliana* have been produced (Supplemental Table 1). A *C. campestris* draft genome assembly with higher contiguity relative to the one used by (Shahid et al., 2018) has also been described (Vogel et al., 2018). The additional small RNA-seq data were used in conjunction with the improved genome assembly to identify interface-induced *MIRNA* loci. A total of 156 *C. campestris* interface-induced *MIRNA* ("ccm-IIM") loci, representing 103 families, were annotated (Supplemental Datasets 1-3). None of these families have been annotated in other plant species (per miRBase version 22). These improved annotations more than triple the known number of ccm-IIM loci, and include all miRNAs previously shown to target host mRNAs. All data are searchable with genome browsers and integrated small RNA visualization tools at https://plantsmallrnagenes.science.psu.edu/Studies/Hudzik.

C. campestris interface-induced miRNAs accumulate prior to host penetration

Whether using *A. thaliana* inflorescence stems or *Solanum lycopersicum* hypocotyls as a host, haustorium organogenesis progressed at the same rate (Supplemental Figures 1-2). Haustoria were in the adhesive phase during days 0-2 of the time-course when the formation of the endophyte primordia was observed (Figures 1A, 1D). The intrusive phase, discerned by searching hyphae invading the host cortex, spanned days 3-5 (Figures 1B, 1E). A xylem bridge connecting host and parasite vasculature via the haustorium was not detectable until day 6 (Figures 1C, 1F); this marks the start of the conductive phase.

sRNA sequencing was performed across a 15 day time-series (days 0-14) of *C. campestris*-host interfaces for both *A. thaliana* and *S. lycopersicum* hosts. Interface-induced miRNAs began accumulating in the adhesive phase, and reached maximum levels by the start of the intrusive phase (Figure 1G, 1H). Interface-induced miRNAs can stimulate the generation of secondary siRNAs following an initial cleavage event on a host transcript (Shahid et al., 2018; Johnson et al., 2019). Appearance of secondary siRNAs must therefore occur after miRNAs interact with host mRNAs. Accumulation of secondary siRNAs did not begin until the intrusive phase, and did not reach maximum levels until the conductive phase (Figure 1G, 1H). These data show that interface-induced miRNAs appear early in haustorial development, before any penetration of host tissue has occurred.

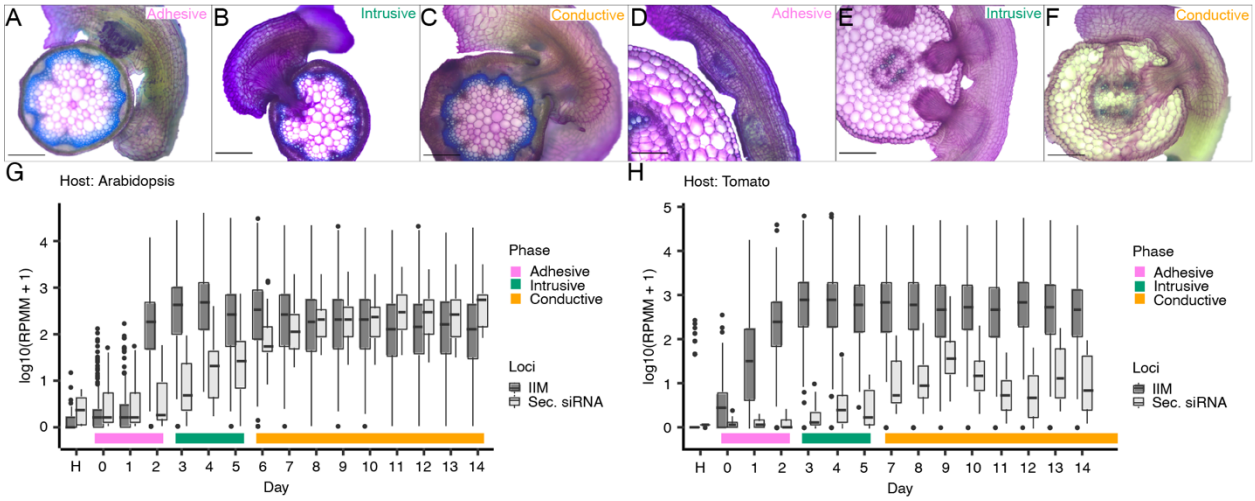

Figure 1: Interface-induced miRNAs are detectable during the adhesive phase. Histological sections of haustoria growing on *A. thaliana* (A-C) and *S. lycopersicum* (D-F). Top right text in each image (A-F) denotes the stage of haustorium organogenesis, the color correlates with the phases labeled in G and H. (Scale bars: 200µm) (G, H) Detection of interface-induced miRNAs (IIM) and secondary siRNAs (Sec. siRNA) using *A. thaliana* or *S. lycopersicum* as hosts. Boxplots show medians (central line), 25th-75th percentiles (box boundaries), up to 1.5x the interquartile range (whiskers), and outliers (dots). RPMM: Reads per million mapped.

C. campestris interface-induced miRNA induction is not host-dependent

C. campestris has a broad host range. One possible method of adapting to diverse hosts could be to adjust interface-induced miRNA accumulation depending on the host species. This hypothesis was tested by plotting the median conductive phase small RNA accumulation levels of each interface-induced *MIRNA* locus from tomato and *A. thaliana* hosts. The resulting plot showed a linear correlation (Figure 2A), where each *MIRNA* locus accumulated miRNAs to similar levels with either species as a host. This argues against the hypothesis that miRNA induction varies depending on the host species.

Detached shoot tips of *C. campestris* can be stimulated to differentiate haustoria by specific light and tactile stimuli (Figure 2B; (Kaga et al., 2020)). These *in vitro* haustoria can be produced either with or without adjacent host tissue, such as detached host leaves (Figure 2B). *In vitro* haustoria produced with or without adjacent *A. thaliana* leaves were processed in triplicate for small RNA sequencing to test interface-induced miRNA accumulation. *C. campestris* shoot tips (also in triplicate) were used as a negative control. Interface-induced miRNAs were abundant in *in vitro* haustoria regardless of the presence or absence of detached host leaves (Figure 2C). Median accumulation levels of individual miRNAs were highly correlated between *in vitro* haustoria produced with or without adjacent host tissue (Figure 2D). These observations demonstrate that *C. campestris* interface-induced miRNA production is independent of any host. Instead, their sudden appearance during early haustorial development is part of an inherent developmental program.

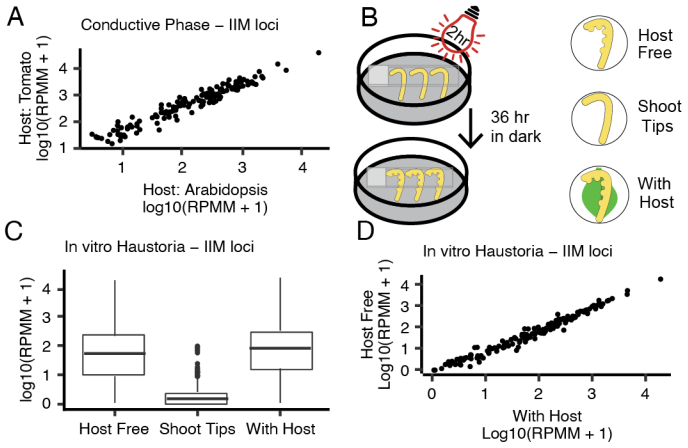

Figure 2: Interface-induced miRNA production is independent of a host. (A) Comparing interface-induced miRNA population and abundance between hosts. Each dot represents the median value of conductive phase samples for an interface-induced miRNA. (B) Graphical overview of *in vitro* haustoria experiment. (C) Interface-induced miRNA accumulation from *in vitro* haustoria. Boxplots show medians (central line), 25th-75th percentiles (box boundaries), up to 1.5x the interquartile range (whiskers), and outliers (dots). (D) Comparing interface-induced accumulation between the Host Free and With Host *in vitro* haustoria. Each dot represents the median value across all replicates for a single microRNA. IIM: Interface-induced microRNA; RPMM: Reads per million mapped.

C. campestris interface-induced *MIRNA* loci share a common upstream sequence element known to control snRNA transcription in plants

Genomic DNA sequences upstream of the ccm-IIM loci were analyzed with MEME (Bailey et al., 2009) to search for over-represented sequence motifs. Transcription start sites for these *MIRNA* primary transcripts were initially unknown, so the ends of the upstream regions were defined by the 5' basal DCL cut site on the *MIRNA* hairpins (Figure 3A). A highly overrepresented ten nucleotide motif was discovered (Figure 3B). This motif, termed the Upstream Sequence Element (USE), was found adjacent to most of the interface-induced *MIRNA* loci (Figure 3C). As a control, a set of "canonical" *MIRNA* loci from *C. campestris* was annotated. These canonical loci encode miRNAs universal among dicots such as miR156, miR164, and miR166. None of the canonical *MIRNA* loci had the USE in their upstream regions (Figure 3C). The motif has a strong tendency to be located ~100 base pairs upstream of the 5' basal DCL cut sites of the interface-induced *MIRNA*s (Figure 3D). A previous study produced nanoPARE data from *C. campestris* / *A. thaliana* haustorial interfaces (Johnson et al., 2019); nanoPARE is an RNA-seq method that captures 5' ends of RNAs. These data were analyzed to find the 5' ends of *MIRNA* primary transcripts. There was a clear peak of nanoPARE data around 40 base-pairs upstream of the 5' basal DCL cut site of the interface-induced *MIRNA*s (Figure 3E). No such peak was apparent when analyzing the canonical *MIRNA* loci (Figure 3E). This analysis suggests that the transcriptional start sites of interface-induced *MIRNA* primary transcripts about 40 bps upstream of the 5'-basal DCL cut site, and thus lie downstream of the USE.

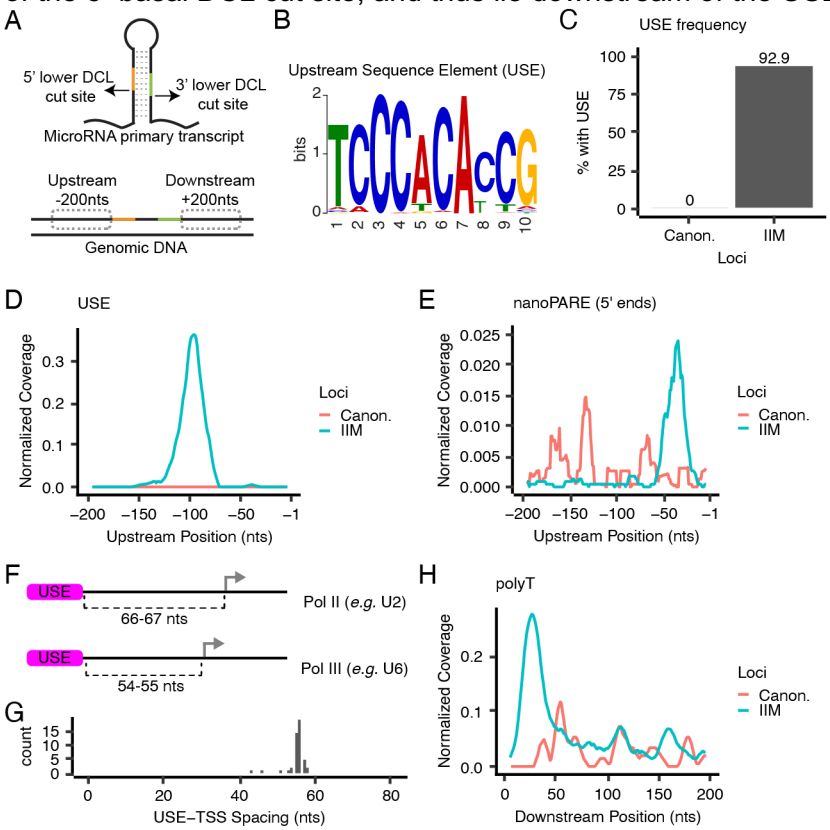

Figure 3: Interface-induced miRNA loci share a *cis*-regulatory element with snRNAs. (A) Schematic showing upstream and downstream regions. (B) MEME sequence logo of the USE found upstream of interface-induced *MIRNA* loci. (C) Presence of the USE at interface-induced miRNA loci and canonical miRNA loci in *C. campestris*. (D) Metaplot of USE coverage as a function of upstream position. (E) Metaplot of normalized nanoPARE 5' end coverage. (F) Distances between USE and transcriptional start sites (arrows) for known USE-dependent Pol II and III type promoters. (G) Frequency distribution of USE-TSS distances for interface-induced miRNAs. (H) Metaplot of polyT coverage (defined as six or more consecutive T residues on the coding strand) in downstream regions. Canon. : Canonical microRNA loci; IIM: Interface-induced microRNA loci; TSS: Transcriptional start site.

206 ***C. campestris* interface-induced *MIRNA* loci have features consistent with RNA**
207 **Polymerase III transcription**
208 The USE found at *C. campestris* interface-induced *MIRNA* loci is identical to a motif known to
209 drive U-snRNA transcription in plants (Vankan and Filipowicz, 1989). U-snRNAs are short non-
210 coding RNAs that, along with associated proteins, form the spliceosome. The spliceosome
211 functions to catalyze intron removal from Pol II-transcribed RNAs during nuclear RNA
212 maturation. The USE is a unique *cis*-regulatory element because it can drive either Pol II or Pol
213 III transcription of U-snRNAs (Waibel and Filipowicz, 1990b). When the USE is 66-67 base-pairs
214 upstream from the transcriptional start site (TSS) it drives Pol II transcription (Figure 3F). When
215 the USE is 54-55 base-pairs upstream of the TSS (one helical turn of DNA shorter), it instead
216 drives Pol III transcription (Figure 3F). *A. thaliana* U2, U4, and U5 snRNA genes contain the
217 longer spacing and are transcribed by Pol II, while *A. thaliana* U6 snRNA genes have the
218 shorter spacing and are transcribed by Pol III (Waibel and Filipowicz, 1990b; Waibel and
219 Filipowicz, 1990a). The TSSs of 48 of the *C. campestris* interface-induced MIRNA primary
220 transcripts were inferred from nanoPARE data (Figure 3E); the rest could not be inferred due to
221 low/no coverage in the nanoPARE data. The USE-TSS distance at these loci had a sharp peak
222 at about 55 base-pairs (Figure 3G), exactly the spacing expected for USE-dependent Pol III
223 transcription. Pol III termination is triggered by runs of T residues on the non-template strand;
224 four Ts is a minimal signal for termination, and six or more Ts are maximally effective (Gao et
225 al., 2018). Runs of six or more T's were common immediately downstream of interface-induced
226 *MIRNA* loci (Figure 3H). The upstream similarity to U6 snRNA promoters and the prevalence of
227 downstream poly-T stretches suggests that *C. campestris* interface-induced *MIRNA* loci could
228 be transcribed by Pol III.
229
230 **Accumulation of interface-induced microRNAs in a heterologous system depends on the**
231 **USE**
232 *Agrobacterium tumefacians* T-DNA vectors containing *C. campestris* interface-induced *MIRNA*
233 loci were constructed (Figure 4A). The T-DNA did not contain any selectable markers to avoid
234 recruitment of RNA polymerases; transcription of these loci depends solely on any *cis* elements
235 present in the *MIRNA* loci. For each *MIRNA* tested a wild-type and USE-scrambled version
236 were prepared. These T-DNA were introduced to *Nicotiana benthamiana* leaf mesophyll cells by
237 Agro-infiltration. Mature miRNA levels were quantified by qRT-PCR. Mature miRNAs
238 accumulated when wild-type loci were introduced (Figures 4B-C). When the USE element was
239 scrambled, mature miRNA accumulation was dramatically lower (Figures 4B-C). This supports
240 the hypothesis that the USE is a *cis*-acting factor that promotes miRNA accumulation. This
241 result also demonstrates the *C. campestris* interface-induced *MIRNA* precursors can be
242 correctly processed by the RNAi machinery of a heterologous host.
243

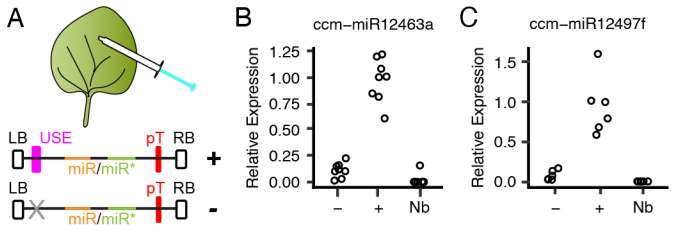

244
245
246 **Figure 4:** The USE is required for accumulation of interface-induced miRNAs during transient expression in *N.*
247 *benthamiana*. (A) Graphical representation of constructs used during transient expression. LB: left border; USE:
248 upstream sequence element; pT: polyT stretch; RB: right border. (B-C) Relative expression of miR12463a or
249 miR12497f with scrambled USE sequence (-), wild-type USE sequence (+), and *N. benthamiana* leaf not infiltrated
250 (Nb). Expression was normalized to miR159. Each dot represents a biological replicate (RNAs from a distinct
251 infiltrated leaf).

Discussion

We observed that *C. campestris* interface-induced miRNAs begin accumulating in the adhesive phase, even before the parasite has penetrated the host stem. This suggests that interface-induced miRNAs are primed for immediate use by developing haustoria. Accumulation of interface-induced miRNAs is fully independent of the host identity, and does not even require any host. This indicates that their accumulation is a programmed aspect of haustorial development. *C. campestris* is a generalist parasite that feeds on a wide range of host plants. This "shotgun" strategy of miRNA accumulation could be well-suited for a generalist that feeds on diverse hosts. This host-insensitive, shotgun strategy is also consistent with earlier observations of *Cuscuta* miRNA polymorphisms that compensate for most possible variations of target sites within host mRNAs (Johnson et al., 2019).

We also found a snRNA-like USE adjacent to nearly all interface-induced miRNA loci. The USE is not found at any canonical miRNA loci in *C. campestris,* and has not been reported at miRNA loci in any other plant. The distance between the USE and transcriptional start sites of interface-induced miRNAs is consistent with U6-like Pol III transcription, as is the presence of potential Pol III terminators immediately downstream of most loci. The USE drives accumulation of miRNAs in a heterologous system, directly demonstrating its function as an activating *cis*-regulatory element. We hypothesize that the *C. campestris* interface-induced miRNA precursors are transcribed by RNA Pol III in a USE-dependent manner. We speculate that the use of Pol III, instead of Pol II, may somehow mark the interface-induced miRNAs for specialized processing and eventual export from the parasite into the host. The interface-induced miRNAs avoid "self-targeting" of *C. campestris* mRNAs (Shahid et al., 2018; Johnson et al., 2019); this is consistent with the hypothesis that they are made for "export only" and not assembled onto *C. campestris* AGO proteins. The accumulation of mature miRNAs in *in vitro* haustoria with no host tissue present directly demonstrates that Dicing of the interface-induced miRNA precursors occurs within *C. campestris*. Therefore the exported molecule is either mature miRNA or the miRNA/miRNA* duplex.

Plant U6 promoters are workhorses for constitutive expression of short non-coding RNAs. For instance, the U6-26 promoter from *A. thaliana* is widely used to drive Pol III-dependent sgRNA expression in CRISPR experiments (Tsutsui and Higashiyama, 2017; Lowder et al., 2018). U6-26 has the same USE as the *C. campestris* interface-induced miRNAs (Waibel and Filipowicz, 1990a). Indeed, the U6 snRNA is often used as a loading control for miRNA blots, including in the first report of interface-induced miRNAs (Shahid et al., 2018). How does the USE, which in all previously known contexts drives constitutive transcription, result in miRNAs with such a tissue-specific accumulation pattern? One hypothesis is constitutive transcription but tissue-specific dicing of the precursors. However RNA blots and RNA-seq experiments have yet to detect any strong precursor accumulation in non-haustorial tissues. Resolving the mystery of highly-specific accumulation from a promoter that is expected to be constitutive will be an important goal for future research.

In summary, we find that the *C. campestris* interface-induced miRNAs are distinguished from canonical miRNAs by a distinct set of genomic sequence features. This implies that these miRNAs are fundamentally distinct from normal miRNAs and siRNAs. The common promoter element suggests a possible avenue for disruption of *trans*-species miRNA activity: targeting the factors that bind USE should reduce production of *trans*-species miRNAs.

Materials and Methods

Annotation of *Cuscuta campestris* interface-induced *MIRNA* loci

303 Annotation of *MIRNA* loci occurred in two steps (early and late) based on the availability of small
304 RNA-seq data during the course of the study. In the early step, previously published small RNA-
305 seq datasets from the interface or parasite stem of *C. campestris* attached to *A. thaliana* were
306 obtained as fastq files from the Sequence Read Archive (SRA; Supplemental Table 1). Trailing
307 3'-sequencing adapters were discovered and trimmed using gsat
308 (https://github.com/MikeAxtell/gsat). Trimmed small RNA datasets were then aligned to the *A.*
309 *thaliana* genome (version TAIR10, including plastid and mitochondrial genomes) using bowtie
310 (Langmead et al., 2009) demanding exact matches and directing unmapped reads to a new
311 fastq file (non-default settings '-v 0 --un'). Small RNA reads that aligned were discarded; this
312 eliminated most small RNAs that could have been produced by the host genome. The remaining
313 reads were analyzed together in a single ShortStack run (version 3.8.5; default settings)
314 (Johnson et al., 2016) using the *C. campestris* genome assembly version 0.32 (Vogel et al.,
315 2018) as the reference genome. This resulted in *de novo* annotation of thousands of discrete
316 small RNA-producing loci. Read counts of aligned small RNAs from each locus in each library
317 were retrieved (from the 'Counts.txt' file produced by ShortStack) and used as input for
318 differential expression analysis using DESeq2 (Love et al., 2014). Differential expression
319 analysis of interface vs. parasite stem was independently performed for each of the three
320 studies included in the first step (Shahid et al. expt.1, Shahid et al. expt. 2, and Johnson et al.;
321 Supplemental Table 1). DESeq2 analysis used 'lfcShrink' using the 'normal' shrinkage estimator;
322 loci up-regulated in interface relative to parasite stem with an FDR-adjusted p-value of < 0.05
323 were called differentially expressed. The union of all three sets of differentially expressed loci
324 from each study was then computed and retained. From these, loci where a) greater than 80%
325 of aligned reads were between 20-24 nucleotides in length and b) the single most abundant
326 aligned RNA size was 20, 21, 22, or 23 nucleotides long were retained. The retained loci were
327 then individually examined using multiple visualization tools: Integrative Genomics Viewer
328 (Robinson et al., 2011), strucVis (https://github.com/MikeAxtell/strucVis), and sRNA_Viewer
329 (https://github.com/MikeAxtell/sRNA_Viewer). Based on the manual examinations, loci that did
330 not conform to all of the guidelines for confident plant *MIRNA* locus annotation (Axtell and
331 Meyers, 2018) were discarded. The late phase of *MIRNA* annotation took advantage of the
332 much greater amount of sRNA-seq data generated during the time-course analyses of *C.*
333 *campestris* on both *A. thaliana* and *S. lycopersicum* hosts (Supplemental Table 1). The same
334 analysis approach was used to identify interface-induced *MIRNA* loci using days 9 and 10 as
335 'Interface' samples and day 0 and "host only" as negative control samples. Loci identified in the
336 late phase were then merged with those obtained in the early phase. All together 156 *C.*
337 *campestris* interface-induced *MIRNA* loci were found (Supplemental Datasets 1-3). These loci
338 and the supporting data can be interactively browsed at
339 https://plantsmallrnagenes.science.psu.edu/Studies/Hudzik.
340
341 The mature 5p-miRNA and 3p-miRNA from each locus was queried against miRBase (version
342 22) mature miRNAs using the SSEARCH function (hosted on the miRBase website), restricting
343 hits to Viridiplantae. The mature 5p-miRNA and 3p-miRNA from each loci were also queried
344 against the "superfamilies" described by (Johnson et al., 2019) using ggsearch36 (from the
345 FASTA package), restricting the search to forward strand hits only; alignments were kept that
346 had less than 3 mismatches. In order to group the loci into families, The mature 5p-miRNA and
347 3p-miRNA from each loci were queried against each other in an all vs. all search using
348 ggsearch36, restricting the search to forward strand hits only. Families were defined by no more

349 than 7 mismatches between a given 5p-miRNA and 3p-miRNA. Based on this analysis the 156
350 loci were grouped into 103 distinct families[1].
351
352 **Plant growth conditions**
353 Host plants grown for time-course experiments, *A. thaliana* (Col-0) and *S. lycopersicum* (IL-8-1-
354 1), were grown at 20-22°C and subjected to 16h photoperiods under fluorescent tube lighting.
355 *C. campestris* seeds were scarified with sulfuric acid for 1 hour, followed by 5-6 washes with
356 water. Scarified seeds were placed in glass petri dishes with moist paper towels and placed in
357 a growth chamber at 28°C with 16h photoperiods under fluorescent tube lighting for 3 days.
358 Emerged seedlings were then transplanted to the base of host plants and supplemented with
359 far-red LED lighting throughout the time-course to allow for attachment.
360
361 **Time-course of *C. campestris* haustoria development**
362 Host plants were grown as described above until inflorescence stems of *A. thaliana* hypocotyls
363 of *S. lycopersicum* were able to serve as hosts for *C. campestris. C. campestris* seedlings were
364 scarified and germinated as described above and were placed at the base of inflorescence
365 stems and hypocotyls under a combination of fluorescent tube lighting and far-red LED lights.
366 Day 0 of the time-course was defined as the day that *C. campestris* had successfully wrapped
367 around a host. Samples were subsequently collected every twenty-four hours. Each day in the
368 time course included three biological replicates consisting of four interfaces. Samples which
369 were used to create sRNA sequencing libraries were flash frozen in liquid nitrogen and stored at
370 -80°C until total RNA extraction was performed using a BioSpec Mini-Beadbeater and Tri-
371 Reagent (Sigma) following the manufacturer's protocol.
372
373 Samples which were subjected to vibratome sectioning were collected and sectioned within the
374 same day. A .stl file created by (Atkinson and Wells, 2017) containing instructions for 3D
375 printing a mold to embed samples in agarose for vibratome sectioning was printed. Interfaces
376 were placed in the mold and embedded in freshly prepared 5% agarose. Once solidified,
377 excess tissue and agarose were trimmed, and the samples were mounted on a metal block
378 using superglue. Mounted samples were secured with a vice grip in the Vibratome 1000 Plus
379 Sectioning System bath. Samples were submerged in ice-cold nanopure water and sectioned
380 with a thickness of 200µm using Personna 3-Facet Double Edge AccuTec Blades at a blade
381 angle of 15°. Sections were stained with freshly prepared 0.002% toluidine blue on a shaker for
382 ten minutes in 3x4 cell culture plates and rinsed 3-4 times with nanopure water. Sections were
383 observed on a Zeiss AXIO Scope A1 trinocular optical microscope using the 10x objective and
384 imaged with a Jenoptik ProgRes C14 Plus microscope CCD. Image processing to remove
385 excess stained agarose from the background was identical for all images. Scale bar of 200µm
386 was added to all images using ImageJ.
387
388 ***In vitro* haustoria**
389 Stimulation of haustorial development in the absence of host tissues was similar to previously
390 described methods (Kaga et al., 2020; Jhu et al., 2021). *C. campestris* was cultivated on beets
391 in a greenhouse. Shoot tips, approximately 6-8 cm in length, were cut and placed on a 3%
392 agarose plate. Unstimulated shoot tips were flash-frozen at this point for later RNA extraction.
393 Shoot tips "with host" included fresh cut rosette leaves from wild-type (Col-0) *A. thaliana* plants

[1] *N.b.* for reviewers and preprint readers: Not all of these annotations are homologs of already described miRBase families, so many don't yet have miRBase-registered numbers. These cases are temporarily named "ccm-IIM", for *Cuscuta campestris* interface-induced *MIRNA*s. Upon acceptance, these will be registered at miRBase, and the final miRBase numbers will be substituted into the datasets during final revisions.

394 pressed on the tips. Shoot tips were stimulated to form haustoria by weighting with ~8 glass
395 cover slips, exposure to a far-red LED bulb for two hours, followed by four days in complete
396 darkness. The resulting haustoria were collected, flash-frozen, and used for RNA extraction.
397 Total RNA was extracted using a bead-beater and Tri-Reagent (Sigma) per the manufacturer's
398 instructions. Three samples per condition, each from a different plate, were collected and
399 extracted.
400
401 **Small RNA sequencing and analysis**
402 All small RNA-seq libraries were constructed using 500ng of total RNA using the splint-ligation
403 method described by (Maguire et al., 2020). Libraries were sequenced on an Illumina NextSeq
404 550 (time-course experiments) or NextSeq 2000 (*in vitro* haustoria experiments). Time-course
405 experiment: After de-multiplexing, FASTQ files were trimmed using cutadapt (Martin, 2011) with
406 settings -a AGATCGGAAGAGCACACGTCTGAAC -m 15 --discard-untrimmed. Two
407 concatenated genomes were prepared: *A. thaliana* TAIR10 and *C. campestris* v0.32, and *S.*
408 *lycopersicum* release 5 and *C. campestris* v0.32. Trimmed reads were aligned to the
409 appropriate concatenated genome using ShortStack (Johnson et al., 2016) version 3.8.5 with
410 setting --align_only. The resulting BAM-formatted alignments were split based on reference
411 genome, to create two BAM files per time-course: One for *C. campestris*, the other for the host
412 genome. These are the alignments hosted at
413 https://plantsmallrnagenes.science.psu.edu/Studies/Hudzik. The *C. campestris* alignments were
414 analyzed using ShortStack version 3.8.5 with a 'locifile' containing the coordinates of all 156
415 interface-induced *MIRNA* loci (Supplemental Dataset 1). The host-genome alignments were
416 similarly analyzed with a 'locifile' containing locations of known secondary siRNA loci triggered
417 by interface-induced miRNAs (Supplemental Table 2). The resulting count matrices, showing
418 alignments by sample, were combined and processed to yield normalized values in units of read
419 per million mapped. Analysis of small RNA-seq from *in vitro* haustoria was identical except that
420 alignments used only the *C. campestris* genome and no secondary siRNA loci were analyzed.
421
422 **Analysis of flanking DNA**
423 Upstream and downstream DNA sequences (200 base-pairs each) flanking the 156 interface-
424 induced *MIRNA* loci were retrieved from the version 0.32 *C. campestris* genome assembly
425 (Vogel et al., 2018). Upstream regions were defined to end at the 5' basal DCL cut site;
426 downstream regions were defined to begin at the 3' basal DCL cut site (Figure 3A). Upstream
427 sequences were analyzed with MEME suite (version 5.4.1) (Bailey et al., 2009). Motif discovery
428 with meme used settings '-dna -mod zoops -nmotifs 1 -w 10 -objfun classic -revcomp -
429 markov_order 0'. The top-scoring motif was then used as a query of the upstream sequences
430 with the MEME suite tool fimo using settings '--qv-thresh --thresh 0.05'; this captured all
431 occurrences of the motif with a false-discovery rate of <= 0.05. In a few cases where the motif
432 was found more than once on the same upstream sequence, only the top-scoring instance was
433 retained. The motif consensus sequence is TCCCACA[CT]CG (Figure 3B). The fimo analysis
434 was also run using the upstream regions of conserved, canonical *MIRNA* loci from *C.*
435 *campestris*; no motif instances were found with an FDR <= 0.05. Motif locations were converted
436 to gff3 format, and then converted to modified gff file with metaplot coordinates based on
437 distance from the 5' basal DCL sites. The subcommand 'genomecov' from the bedtools suite
438 (Quinlan and Hall, 2010) was then used with option -d to calculate position-specific depths.
439 These values were then normalized by dividing by the number of loci in each set (interface-
440 induced *MIRNA* loci or conserved canonical *MIRNA* loci). Moving averages with a window size
441 of 10 were then plotted (Figure 3D). Downstream regions were searched for stretches of six or
442 more T nucleotides on the *MIRNA* coding strand; locations were converted to gff3 format and
443 processed as described above to create metaplots (Figure 3H).
444

445 **NanoPARE analysis and transcriptional start site inference**
446 Previously described nanoPARE data (Johnson et al., 2019) from *C. campestris* haustorial
447 interfaces with *A. thaliana* stems were retrieved in FASTQ format from the Sequence Read
448 Archive (SRA): Accessions SRR9216111, SRR9216113, and SRR9216114. Contaminating
449 adapter sequences were removed using cutadapt (Martin, 2011) with settings -a
450 CCGAGCCCACGAGACTAAGGCGAATCTCGTATGCCGTCTTCTGCTTG -a
451 CCGAGCCCACGAGACCGTACTAGATCTCGTATGCCGTCTTCTGCTTG -a
452 CCGAGCCCACGAGACAGGCAGAAATCTCGTATGCCGTCTTCTGCTTG -a
453 CCGAGCCCACGAGACGGACTCCTATCTCGTATGCCGTCTTCTGCTTG -a
454 CCGAGCCCACGAGACTAGGCATGATCTCGTATGCCGTCTTCTGCTTG --trim-n -m 20.
455 Trimmed reads were aligned to the version 0.32 *C. campestris* genome assembly (Vogel et al.,
456 2018) using STAR (Dobin et al., 2013) with settings --outFilterMismatchNmax 999 --
457 outFilterMismatchNoverReadLmax 0.07 --outWigType wiggle read1_5p --outWigNorm None.
458 The two resulting .wiggle formatted files contained the depths of RNA 5' ends genome-wide;
459 these files were converted to bigwig format using wigToBigWig (Kent et al., 2010). The bigwig
460 files were then queried to retrieve data from the 200 base-pair upstream regions of each of the
461 interface-induced *MIRNA* loci and each of the conserved canonical *MIRNA* loci using
462 bigWigToBedGraph (Kent et al., 2010). The read depths for each locus were scaled by reads /
463 total reads; this scaled the data so that each locus had equal weight. Actual coordinates were
464 converted to metaplot coordinates based on distance from 5' basal DCL sites. Scaled depths
465 were normalized by dividing by the number of loci in each set (interface-induced *MIRNA* loci or
466 conserved canonical *MIRNA* loci). Moving averages with a window size of 10 were then plotted
467 (Figure 3E). Transcriptional start sites of interface-induced *MIRNA* primary transcripts were
468 inferred to be the maximum nanoPARE read depth location in the 200 base-pair upstream
469 regions; ties were broken randomly.
470
471 **Agroinfiltration of interface-induced *MIRNA* loci**
472 Synthetic double-stranded DNA fragments based on the genomic sequences of two *C.*
473 *campestris* interface-induced *MIRNA* loci were synthesized: ccm-*MIR12463a* and ccm-
474 *MIR12497f*. Two versions of each were constructed: wild-type, and a version where the ten
475 base-pair USE was randomly scrambled. Synthetic DNA fragments were golden-gate cloned
476 into vector pGGZ001 (Lampropoulos et al., 2013) using sites 'A' and 'G'. The T-DNA regions
477 were confirmed by Sanger sequencing. Complete plasmid sequences are in Supplemental
478 Dataset 4. Plasmids were transformed into *Agrobacterium tumefacians* GV3101-pMP90-pSoup.
479 Agroinfiltration into *Nicotiana benthamiana* leaves was performed as previously described (Liu
480 et al., 2014). Leaf samples from infiltrated areas were collected four days after infiltration and
481 processed for total RNA extraction. Total RNA was extracted using one of the following
482 methods: Tri-Reagent (Sigma), New England Biolabs Monarch Total RNA Miniprep Kit (T2010),
483 or Zymo Quick-RNA Plant Miniprep kit (R2024). RNA samples were diluted to 100ng/ul, and
484 used in stem-loop reverse-transcription reactions (Yang et al., 2014) using primers specific to
485 the target miRNA, and to miR159 (which served as a reference gene). Stem-loop reverse
486 transcription primers were self-annealed at 100uM concentration in IDT Duplex Buffer (100mM
487 potassium acetate, 30mM HEPES pH7.5) by heating in a 94C heat block for two minutes
488 followed by de-activation of the heat block for slow cooling to room temperature. Self-annealed
489 primers were diluted to 50nM stocks in water and stored at –20C. Reverse transcription
490 reactions contained 4ul total RNA (at 100ng/ul), 2ul of a freshly prepared stem-loop primer
491 mixture that had each primer at 5nM concentration, 2ul of 5X reverse transcriptase buffer, 1ul of
492 100mM DTT, 0.5ul of 10mM dNTP, and 0.5ul of Protoscript II reverse transcriptase (New
493 England Biolabs M0368). Reverse transcription reactions were incubated at 16C for 20 minutes,
494 42C for 60 minutes, and 80C for five minutes. 1.5ul of the resulting cDNA was used as template
495 in 20ul scale qPCR reactions using Luna Universal qPCR master mix (New England Biolabs

M3003) with forward primers specific to the microRNA of interest and a universal reverse primer. PCR conditions for miR12463 detection were 95C for 60 seconds (initial denaturation), 95C 5 seconds (denature), 55C 15 seconds (anneal), 70C 10 seconds (extend and detect). PCR conditions for miR12497 detection were 95C for 60 seconds (initial denaturation), 95C 15 seconds (denature), 52C 15 seconds (anneal), 72C 30 seconds (extend and detect). Reaction efficiencies for each miRNA were calculated by serial dilution of positive cDNA samples. Efficiency-corrected accumulation relative to miR159 was calculated using the method of (Pfaffl, 2001). Primer sequences are in Supplemental Table 3.

Data Sharing Plan

Newly created small RNA-seq data have been deposited at NCBI GEO under accessions GSE184641, GSE184642, and GSE205256. Accession numbers for each specific library analyzed are in Supplemental Table 1. Small RNA-seq and associated data are posted on genome browsers with embedded microRNA visualization tools at https://plantsmallrnagenes.science.psu.edu/Studies/Hudzik. Critical datasets are provided in Supplemental Datasets 1-4.

Author Contributions

MJA and CH conceived the project and planned the experiments. MJA and CH conducted most experiments, analyzed data, crafted figures, and wrote the manuscript. SM and SG performed small RNA sequencing. JH made the initial discovery of the upstream sequence element.

Conflict of Interest

SM and SG are employees of New England Biolabs, Inc. New England Biolabs is a manufacturer and vendor of molecular biology reagents, including several enzymes and buffers used in this study. This affiliation does not affect the authors' impartiality, adherence to journal standards and policies, or availability of data. CH, JH, and MJA declare no conflicts of interest.

Acknowledgements

We thank the Huck Institutes Genomics Core Facility for small RNA-seq support and Shawn Burghard for Greenhouse services. This research was supported by awards to MJA from the US National Science Foundation (Award # 2003315) and from the US Department of Agriculture – National Institute of Food and Agriculture (Award # 2018-67013-285).

Supplemental Tables (all in a single Excel file)

Supplemental Table 1. Small RNA-seq datasets used in this study.

Supplemental Table 2. Secondary siRNA loci in tomato and *A. thaliana*.

Supplemental Table 3. Oligonucleotide sequences

Supplemental Datasets

Supplemental Dataset 1. Annotations of *Cuscuta campestris* interface-induced *MIRNA* loci. Includes mature microRNAs and stem-loop precursors. Reference genome is assembly version 0.32 from (Vogel et al., 2018), retrieved from https://plabipd.de/project_cuscuta2/start.ep Format: general feature format version 3 (gff3).

Supplemental Dataset 2. *C. campestris* interface-induced *MIRNA* hairpin sequences. Format: FASTA.

547
548 **Supplemental Dataset 3.** *C. campestris* interface-induced mature miRNA sequences. Both the
549 5p and 3p miRNAs are included for each locus. These are the actually sequenced miRNA
550 sequences; in a few cases there are polymorphisms between the actual sequences and the
551 corresponding sequence in the reference genome. This likely reflects polymorphisms between
552 the strain of *C. campestris* used in this study relative to the reference genome specimen.
553 Format: FASTA.
554
555 **Supplemental Dataset 4**. Sequences and annotations of interface-induced *MIRNA* vectors
556 used in agroinfiltration. Genbank flatfile format (text).
557
558 **Supplemental Figures**

Supplemental Figure 1. *C. campestris* growth on *A. thaliana* stems. Cross-sections of toludine blue stained vibratome sections for days 0-15 following parasite coiling. Scale bars: 200µm.

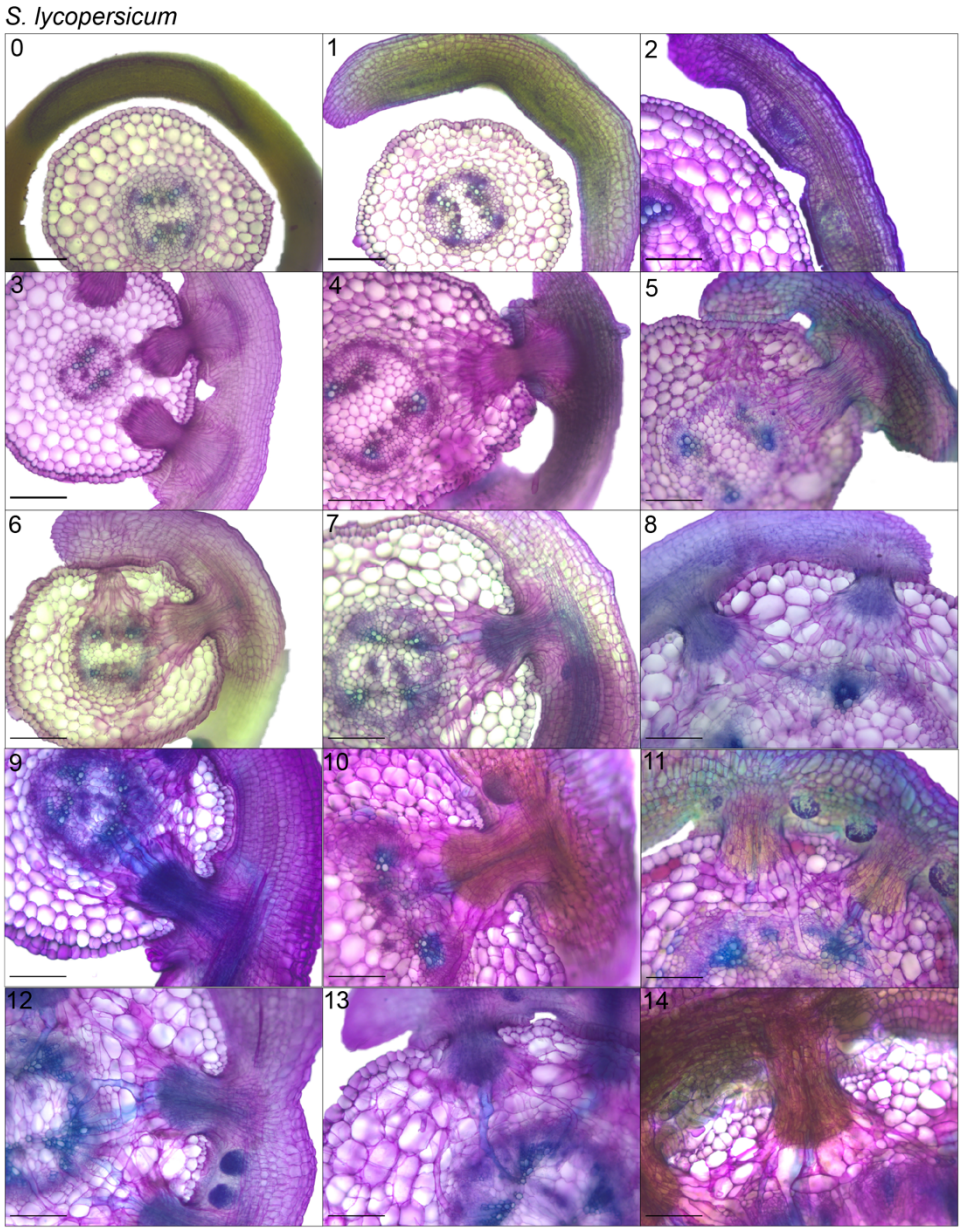

Supplemental Figure 2. *C. campestris* growth on *S. lycopersicum* hypocotyls. Cross-sections of toludine blue stained vibratome sections for days 0-15 following parasite coiling. Scale bars: 200µm.

References Cited

Atkinson JA, Wells DM (2017) An Updated Protocol for High Throughput Plant Tissue Sectioning. Front Plant Sci **8**: 1721

Axtell MJ (2013) Classification and comparison of small RNAs from plants. Annual review of plant biology **64**: 137–159

Axtell MJ, Meyers BC (2018) Revisiting Criteria for Plant MicroRNA Annotation in the Era of Big Data. The Plant cell **30**: 272–284

Bailey TL, Boden M, Buske FA, Frith M, Grant CE, Clementi L, Ren J, Li WW, Noble WS (2009) MEME SUITE: tools for motif discovery and searching. Nucleic Acids Res **37**: W202-208

Birschwilks M, Haupt S, Hofius D, Neumann S (2006) Transfer of phloem-mobile substances from the host plants to the holoparasite Cuscuta sp. Journal of Experimental Botany **57**: 911–921

Cai Q, Qiao L, Wang M, He B, Lin F-M, Palmquist J, Huang S-D, Jin H (2018) Plants send small RNAs in extracellular vesicles to fungal pathogen to silence virulence genes. Science **360**: 1126–1129

Chen H-M, Chen L-T, Patel K, Li Y-H, Baulcombe DC, Wu S-H (2010) 22-Nucleotide RNAs trigger secondary siRNA biogenesis in plants. Proceedings of the National Academy of Sciences of the United States of America **107**: 15269–15274

Chen X (2005) MicroRNA biogenesis and function in plants. FEBS Lett **579**: 5923–5931

Cuperus JT, Carbonell A, Fahlgren N, Garcia-Ruiz H, Burke RT, Takeda A, Sullivan CM, Gilbert SD, Montgomery TA, Carrington JC (2010) Unique functionality of 22-nt miRNAs in triggering RDR6-dependent siRNA biogenesis from target transcripts in Arabidopsis. Nature structural & molecular biology **17**: 997–1003

David-Schwartz R, Runo S, Townsley B, Machuka J, Sinha N (2008) Long-distance transport of mRNA via parenchyma cells and phloem across the host–parasite junction in Cuscuta. The New phytologist **179**: 1133–1141

Dobin A, Davis CA, Schlesinger F, Drenkow J, Zaleski C, Jha S, Batut P, Chaisson M, Gingeras TR (2013) STAR: ultrafast universal RNA-seq aligner. Bioinformatics **29**: 15–21

Fei Q, Xia R, Meyers BC (2013) Phased, secondary, small interfering RNAs in posttranscriptional regulatory networks. The Plant cell **25**: 2400–2415

Gao Z, Herrera-Carrillo E, Berkhout B (2018) Delineation of the Exact Transcription Termination Signal for Type 3 Polymerase III. Molecular Therapy - Nucleic Acids **10**: 36–44

Heide-Jørgensen H (2008) Parasitic flowering plants. doi: 10.1163/ej.9789004167506.i-438

605 **Hou Y, Zhai Y, Feng L, Karimi HZ, Rutter BD, Zeng L, Choi DS, Zhang B, Gu W, Chen X,**
606 **Ye W, Innes RW, Zhai J, Ma W** (2019) A Phytophthora Effector Suppresses Trans-
607 Kingdom RNAi to Promote Disease Susceptibility. Cell Host & Microbe **25**: 153-165.e5

608 **Huang C-Y, Wang H, Hu P, Hamby R, Jin H** (2019) Small RNAs - Big Players in Plant-Microbe
609 Interactions. Cell Host Microbe **26**: 173–182

610 **Hudzik C, Hou Y, Ma W, Axtell MJ** (2020) Exchange of small regulatory RNAs between plants
611 and their pests. Plant Physiol **182**: 51–62

612 **Jhu M-Y, Ichihashi Y, Farhi M, Wong C, Sinha NR** (2021) *LATERAL ORGAN BOUNDARIES*
613 *DOMAIN 25* functions as a key regulator of haustorium development in dodders. Plant
614 Physiology **186**: 2093–2110

615 **Johnson NR, dePamphilis CW, Axtell MJ** (2019) Compensatory sequence variation between
616 trans-species small RNAs and their target sites. eLife **8**: e49750

617 **Johnson NR, Yeoh JM, Coruh C, Axtell MJ** (2016) Improved placement of multi-mapping
618 small RNAs. G3 (Bethesda, Md) **6**: 2103–2111

619 **Kaga Y, Yokoyama R, Sano R, Ohtani M, Demura T, Kuroha T, Shinohara N, Nishitani K**
620 (2020) Interspecific Signaling Between the Parasitic Plant and the Host Plants Regulate
621 Xylem Vessel Cell Differentiation in Haustoria of Cuscuta campestris. Front Plant Sci **11**:
622 193

623 **Kent WJ, Zweig AS, Barber G, Hinrichs AS, Karolchik D** (2010) BigWig and BigBed:
624 enabling browsing of large distributed datasets. Bioinformatics **26**: 2204–2207

625 **Kim G, Westwood JH** (2015) Macromolecule exchange in Cuscuta-host plant interactions.
626 Current opinion in plant biology **26**: 20–25

627 **Lampropoulos A, Sutikovic Z, Wenzl C, Maegele I, Lohmann JU, Forner J** (2013)
628 GreenGate---a novel, versatile, and efficient cloning system for plant transgenesis. PLoS
629 ONE **8**: e83043

630 **Langmead B, Trapnell C, Pop M, Salzberg SL** (2009) Ultrafast and memory-efficient
631 alignment of short DNA sequences to the human genome. Genome biology **10**: R25

632 **Liu Q, Wang F, Axtell MJ** (2014) Analysis of complementarity requirements for plant microRNA
633 targeting using a Nicotiana benthamiana quantitative transient assay. The Plant cell **26**:
634 741–753

635 **Love MI, Huber W, Anders S** (2014) Moderated estimation of fold change and dispersion for
636 RNA-seq data with DESeq2. Genome biology **15**: 550

637 **Lowder LG, Malzahn A, Qi Y** (2018) Plant Gene Regulation Using Multiplex CRISPR-dCas9
638 Artificial Transcription Factors. Methods in molecular biology (Clifton, NJ) **1676**: 197–214

639 **Maguire S, Lohman GJS, Guan S** (2020) A low-bias and sensitive small RNA library
640 preparation method using randomized splint ligation. Nucleic Acids Research gkaa480

641 **Martin M** (2011) Cutadapt removes adapter sequences from high-throughput sequencing reads.
642 EMBnet. journal

643 **Matzke MA, Mosher RA** (2014) RNA-directed DNA methylation: an epigenetic pathway of
644 increasing complexity. Nature reviews Genetics **15**: 394–408

645 **Pfaffl MW** (2001) A new mathematical model for relative quantification in real-time RT-PCR.
646 Nucleic acids research **29**: e45

647 **Quinlan AR, Hall IM** (2010) BEDTools: A flexible suite of utilities for comparing genomic
648 features. Bioinformatics **26**: 841–2

649 **Robinson JT, Thorvaldsdóttir H, Winckler W, Guttman M, Lander ES, Getz G, Mesirov JP**
650 (2011) Integrative genomics viewer. Nat Biotechnol **29**: 24–26

651 **Roney JK, Khatibi PA, Westwood JH** (2007) Cross-species translocation of mRNA from host
652 plants into the parasitic plant dodder. Plant physiology **143**: 1037–1043

653 **Shahid S, Kim G, Johnson NR, Wafula E, Wang F, Coruh C, Bernal-Galeano V, Phifer T,**
654 **dePamphilis CW, Westwood JH, Axtell MJ** (2018) MicroRNAs from the parasitic plant
655 Cuscuta campestris target host messenger RNAs. Nature **553**: 82–85

656 **Shimizu K, Aoki K** (2019) Development of Parasitic Organs of a Stem Holoparasitic Plant in
657 Genus Cuscuta. Front Plant Sci **10**: 1435

658 **Subhankar B, Yamaguchi K, Shigenobu S, Aoki K** (2021) *Trans*-species small RNAs move
659 long distances in a parasitic plant complex. Plant Biotechnology **38**: 187–196

660 **Tsutsui H, Higashiyama T** (2017) pKAMA-ITACHI Vectors for Highly Efficient CRISPR/Cas9-
661 Mediated Gene Knockout in Arabidopsis thaliana. Plant Cell Physiol **58**: 46–56

662 **Vankan P, Filipowicz W** (1989) A U-snRNA gene-specific upstream element and a -30 'TATA
663 box' are required for transcription of the U2 snRNA gene of Arabidopsis thaliana. The
664 EMBO Journal **8**: 3875–3882

665 **Vaughn KC** (2003) Dodder hyphae invade the host: a structural and immunocytochemical
666 characterization. Protoplasma **220**: 189–200

667 **Vaughn KC** (2006) Conversion of the Searching Hyphae of Dodder into Xylic and Phloic
668 Hyphae: A Cytochemical and Immunocytochemical Investigation. International Journal of
669 Plant Sciences **167**: 1099–1114

670 **Vogel A, Schwacke R, Denton AK, Usadel B, Hollmann J, Fischer K, Bolger A, Schmidt**
671 **MH-W, Bolger ME, Gundlach H, Mayer KFX, Weiss-Schneeweiss H, Temsch EM,**
672 **Krause K** (2018) Footprints of parasitism in the genome of the parasitic flowering plant
673 Cuscuta campestris. Nature communications **9**: 2515

674 **Waibel F, Filipowicz W** (1990a) U6 snRNA genes of Arabidopsis are transcribed by RNA
675 polymerase III but contain the same two upstream promoter elements as RNA
676 polymerase II-transcribed U-snRNA genes. Nucleic acids research **18**: 3451–3458

677 **Waibel F, Filipowicz W** (1990b) RNA-polymerase specificity of transcription of Arabidopsis U
678 snRNA genes determined by promoter element spacing. Nature **346**: 199

679 **Weiberg A, Wang M, Lin F-M, Zhao H, Zhang Z, Kaloshian I, Huang H-D, Jin H** (2013)
680 Fungal small RNAs suppress plant immunity by hijacking host RNA interference
681 pathways. Science (New York, NY) **342**: 118–123

682 **Xie Z, Allen E, Fahlgren N, Calamar A, Givan SA, Carrington JC** (2005) Expression of
683 Arabidopsis MIRNA genes. Plant physiology **138**: 2145–2154

684 **Yang L, Wang S, Tang L, Liu B, Ye W, Wang L, Wang Z, Zhou M, Chen B** (2014) Universal
685 stem-loop primer method for screening and quantification of microRNA. PloS one **9**:
686 e115293

687 **Zhang T, Zhao Y-L, Zhao J-H, Wang S, Jin Y, Chen Z-Q, Fang Y-Y, Hua C-L, Ding S-W,**
688 **Guo H-S** (2016) Cotton plants export microRNAs to inhibit virulence gene expression in
689 a fungal pathogen. Nature Plants **2**: 16153

690